COMMUNICATION

Efficiency Enhancement of GaAs Photovoltaics Employing Antireflective Indium Tin Oxide Nanocolumns

By *Peichen Yu,* Chia-Hua Chang, Ching-Hua Chiu, Chin-Sheng Yang, Jue-Chin Yu, Hao-Chung Kuo, Shih-Hsin Hsu,* and *Yia-Chung Chang*

Global-warming issues coupled with high oil prices have become a major driving force for the use of advanced solar power technology, where a key component lies in the development of high-efficiency and low-cost photovoltaic cells. Next generation photovoltaics, hence, demand an efficiency-boosting mechanism in order to render solar energy cost competitive with conventional sources of electricity.[1] Fundamentally, the conversion efficiency of a solar cell depends on the photon absorption, carrier separation, and carrier collection.[2,3] Therefore, an effective antireflection (AR) coating, minimized recombination loss, and good Ohmic contacts are particularly important. Metal grids that inevitably block the transmission of solar energy also require optimization in order to reduce the series resistance. The trade-off between the electrode and the AR coating areas is one of the efficiency-limiting factors in a conventional solar cell.

The conventional AR coating is usually composed of a quarter wavelength stack of dielectrics with different refractive indices. Broad angular and spectral AR is achievable at the price of multiple layers.[4–7] Over the past few years, versatile sub-wavelength structures (SWS) have emerged as promising candidates for AR coatings, due to the characteristics of zero-order gratings, or the so-called moth-eye effects.[8–14] However, the fabrication costs, which involve either electron-beam (e-beam) lithography or various etching processes, can be significant. In addition, the resulting surface-recombination loss due to dry or wet etching could further hinder the applications of SWS in commercial solar cells. Recently, multiple studies have been carried out on indium tin oxide (ITO), titanium dioxide (TiO_2), and silicon dioxide (SiO_2) nanostructures employing oblique-angle deposition methods,[15–17] where the refractive indices of the nanoporous materials can be engineered by adjusting the air volume ratio. Still, the materials require multiple layers to effectively suppress the Fresnel reflection.

[*] Prof. P. Yu, C.-H. Chang, C.-H. Chiu, C.-S. Yang, J.-C. Yu, Prof. H.-C. Kuo
Department of Photonics
and Institute of Electro-Optical Engineering
National Chiao-Tung University
1001 Ta Hsueh Road, Hsinchu
300 Taiwan, (ROC)
E-mail: yup@faculty.nctu.edu.tw
Dr. S.-H. Hsu, Dr. Y.-C. Chang
Research Center for Applied Sciences
Academia Sinica
128 Academia Rd., Sec. 2 Nankang
Taipei 115, Taiwan, (ROC)

DOI: 10.1002/adma.200802563

In this paper, we demonstrate a practical photovoltaic application of ITO nanocolumns serving as a conductive AR layer for GaAs solar cells. As in standard GaAs cells, the use of a nanostructured AR layer could be otherwise limited due to severe front-surface recombination. The characteristic ITO nanocolumns, prepared by glancing-angle deposition with an incident nitrogen flux, offer omnidirectional and broad-band AR properties for both s- and p-polarizations, up to an incidence angle of 70° for the 350–900 nm wavelength range. Calculations based on a rigorous coupled-wave analysis (RCWA) method indicate that the superior AR characteristics arise from the tapered column profiles, which collectively function as a graded-refractive-index layer. The conversion efficiency of the GaAs solar cell with the nanocolumn AR layer increases by 28% compared to a cell without any AR treatment. Moreover, nearly 42% enhancement is achieved for photocurrents generated at wavelengths that are transparent to the window layer.

Figure 1a shows the epitaxial structure of a conventional, single-junction GaAs/AlGaAs solar cell. After the standard fabrication process, the ITO-nanocolumn structure was deposited onto the p-type $Al_{0.8}Ga_{0.2}As$ window layer using glancing-angle e-beam deposition, followed by a post annealing process at 350 °C for 25 min to improve the transmittance. The fabricated device is schematically illustrated in Figure 1b. Glancing-angle deposition has been employed for preparing microscale and nanoscale porous materials based on nucleation formation and self-shadowing effect. However, the characteristic ITO nanocolumn structure seen in this work is rather unique, where the formation involves either catalyst-free or self-catalyzed vapor–liquid–solid (VLS) growth assisted by the introduced nitrogen. The substrate is tilted at a deposition angle of 70° with respect to the incident vapor flux, where the chamber pressure is controlled at 1.33×10^{-2} Pa. As shown in Figure 2a, the initial column formation on a silicon substrate is fairly straight with a diameter of ~50 nm, and the vertical growth does not adopt any specific direction. However, as shown in Figure 2b and c, the ITO columns become uniformly oriented at the end of deposition, following the direction of the incident vapor flux. The columns also become thicker (~100 nm), with a thinner tip ~30 nm in diameter, and resemble tilted cones with a total length of 1.2 μm and a density of $\sim 5 \times 10^9$ cm^{-2}. This tapered-column profile is important to the reflective characteristics of the nanostructured ITO layer. Figure 2d shows that a layer of uniformly-distributed nanocolumns can be prepared in single-step deposition up to an area of 2 cm × 3 cm.

The transmission electron microscopy (TEM) image shown in Figure 2e reveals the core/shell structure of an ITO nanocolumn.

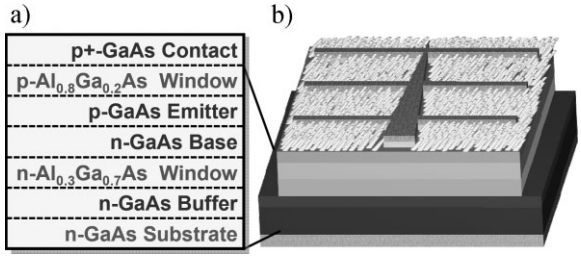

Figure 1. a) Epitaxial structure of a single-junction GaAs solar cell. b) Schematic of a GaAs solar cell fabricated employing ITO nanocolumns as the conductive AR coating.

Energy-dispersive X-ray analyses show that the outer shell has a higher tin content than the core region, indicating the occurrence of tin-doped indium segregation. No apparent catalyst is observed. In addition, the stripe-like Moiré fringes suggest possible material dislocations or composition variations. Presumably, during the initial formation of nucleation cores, the introduced nitrogen facilitates the segregation of tin-doped indium, due to limited availability of oxygen atoms. Due to high substrate temperatures, the liquid-phase nucleation cores have a large accommodation coefficient to promote the absorption of indium oxide and tin oxide vapors, leading to high growth rates. During this phase, the growth direction should be fairly random. Since surface diffusion determines the growth rate and the incident vapor flux determines the amount of atoms that could reach the surface,[18] only those columns that interact with the vapor flux the most can continue the VLS growth, resulting in preferential column formation. Similar formation mechanisms have been reported for ITO whiskers grown by sputtering and by an electron-shower method.[19,20] Finally, it is also believed that the incorporation of oxygen and oxygen vacancies are highly related to optical transmittance and resistivity of the ITO nanocolumns. The sheet resistance of our samples can vary from tens to a few hundred ohms per square, depending on the nitrogen flow rate.[21]

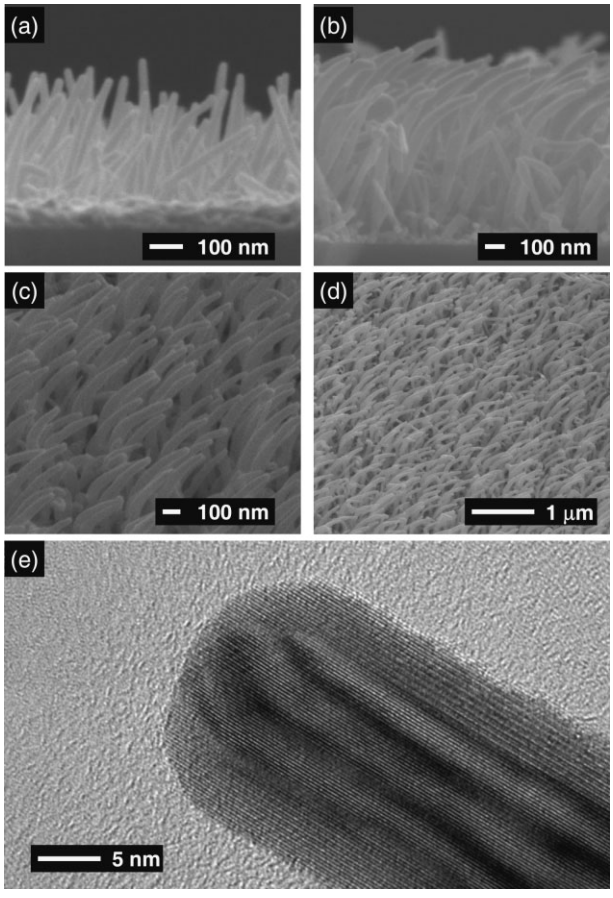

Figure 2. SEM images of ITO nanocolumns deposited with obliquely incident nitrogen flux: a) cross-sectional view of the initial column formation, where the vertical growth direction is fairly random; b) cross-sectional view of the oriented columns at the end of deposition; c) tilted top view of the columns, showing tapered column profiles; d) uniformly distributed nanocolumns that can be prepared in single-step deposition, up to an area of 2 cm ×3 cm. e) TEM image of an ITO nanocolumn, showing a core/shell structure.

The reflectance spectroscopy of ITO nanocolumns grown on a silicon substrate was performed for both s- and p-polarizations, using an ellipsometer with a xenon lamp and monochromator for wavelengths between 350 and 900 nm (V-VASE by J. A. Woollam, Inc.). Both the angle of incidence (AOI), θ_i, and the angle of reflection, θ_o, were varied from 20° to 80°. The system was calibrated with a silicon substrate before each measurement, where the reflectivity was ~35% for the 633 nm wavelength at normal incidence. We also experimentally verified that the reflectivities contributed by high-order diffractions were negligible by fixing θ_i and scanning θ_o on the plane of incidence. The measured angle-dependent reflection characteristics for ITO nanocolumns at 632.8 nm wavelength are shown in Figure 3a for both s- and p-polarizations. As shown in Figure 3a, the reflectivities of ITO-nanocolumn structures have been drastically reduced, showing excellent AR characteristics (<6%) up to an incidence angle of 70° and 80° for s- and p-polarizations, respectively. Such a wide angle of incidence for both polarizations is very beneficial for photovoltaics without an incorporated tracking system. It was also found that the reflection characteristics of the nanocolumn layer do not resemble those of a homogeneous thin film and, hence, an effective refractive index cannot be approximated by curve fitting. To study the correlation between the measured reflection characteristics with the microscopic column profiles, an algorithm based on a RCWA method has been developed to theoretically investigate the reflectivities of ITO nanocolumns. This approach has been successfully applied to GaN nanorods and Si nanopyramids in the past.[22,23] The structural parameters of nanocolumns, such as dimensions and densities, are extracted from the scanning electron microscopy (SEM) images shown in Figure 2b and c. The material dispersion of ITO is also taken into account for absorptions in the ultraviolet wavelength regime (λ<400 nm).[24,25] The inset of Figure 3a illustrates the simulated index profile of a unit cell, consisting of 7 × 7 randomly positioned, tilted pillars defined in an area of 1 μm × 1 μm. As also shown in Figure 3a, the calculated angular reflectivities of ITO nanocolumns agree reasonably well with the measurement for both polarizations. Calculations indicate that the tapered-column profiles contribute to the AR by collectively functioning as

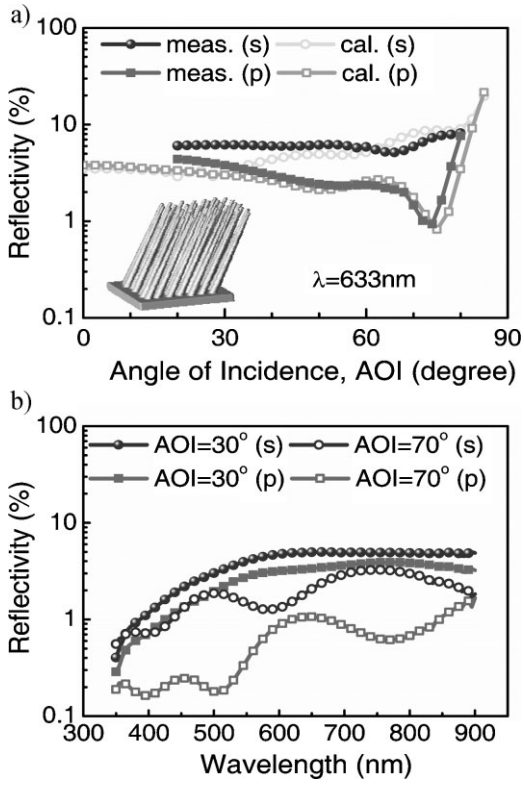

Figure 3. a) The measured and calculated reflectivities of highly oriented ITO nanocolumns are plotted as a function of incidence angle for both s- and p-polarizations at 632.8 nm wavelength. The inset shows the simulated index profile of a unit cell, consisting of 7×7 randomly positioned, tilted columns in an area of $1\,\mu m \times 1\,\mu m$. b) Measured reflection spectroscopy at incidence angles of 30° and 70° for both polarizations in the 350–900 nm wavelength range.

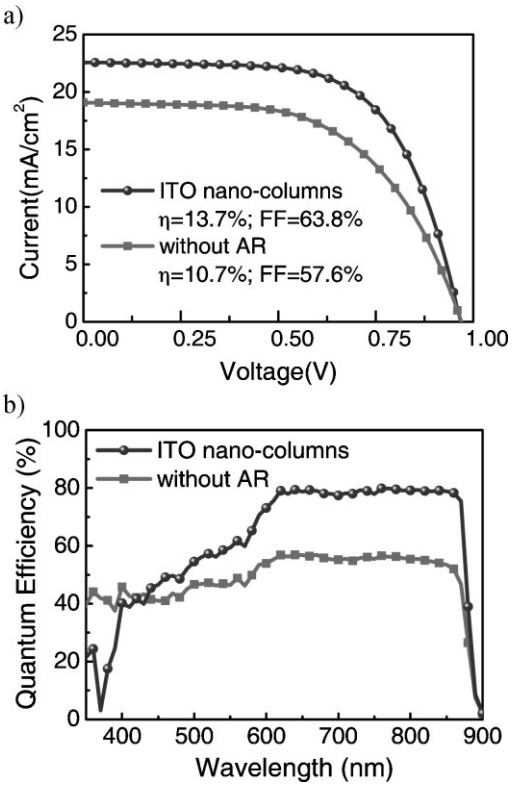

Figure 4. a) Measured *I–V* characteristics of the GaAs solar cell with ITO nanocolumns, compared to a cell without any AR treatment. The overall conversion efficiency is enhanced by 28%. b) Corresponding EQEs, where the efficiencies for both cells deteriorate at wavelengths below 620 nm, mainly due to the $Al_{0.8}Ga_{0.2}As$ window layer.

a graded-index layer. A further reduction in reflectivities is therefore possible via nanocolumns with a larger base diameter. Moreover, the measured spectral reflectivities of ITO nanocolumns shown in Figure 3b confirm the broad-band AR for both AOI = 30° and 70°. The reduced reflection at short wavelengths is also an attribute of graded-index AR coatings. At large incidence angles, the nanostructured ITO behaves as an optically flat thin film, where the interference between the air/ITO and the ITO/Si interfaces can be observed. Similar characteristics have also been verified in calculation. Finally, it is worth noting that although the ellipsometry spectroscopy was taken from the nanocolumns deposited on a silicon substrate, those deposited on the $Al_{0.8}Ga_{0.2}As$ window layer of an actual GaAs cell exhibited equally low reflection characteristics (<6%) for the entire wavelength range of 350–900 nm at normal incidence. Since the nanostructured ITO layer behaves as an effective medium with gradient optical properties, the index difference between $Al_{0.8}Ga_{0.2}As$ and silicon only modifies the overall gradient index profile slightly, and hence, the resulting differences in the respective reflection spectra are negligible.

The GaAs solar cell with ITO nanocolumns was characterized under the AM 1.5g illumination condition and also compared to an identical cell without any AR treatment. The measured current–voltage (*I–V*) characteristics are plotted in Figure 4a. The short-circuit current is enhanced by 18% due to the nanostructured ITO layer, while the fill-factor also increases by 11%, indicating an improved series resistance. Overall, the conversion efficiency is enhanced by 28% with the ITO nanocolumn AR layer. Nonetheless, the external quantum efficiency (EQE) measurement, shown in Figure 4b, indicates that the efficiencies for both cells deteriorate at wavelengths below 620 nm, which is mainly limited by the $Al_{0.8}Ga_{0.2}As$ window layer. The $Al_{0.8}Ga_{0.2}As$ layer has a bandgap of 2.012 eV,[26] corresponding to 616 nm in wavelength. Carriers generated at shorter wavelengths, therefore, suffer from significant surface recombination due to high absorption in GaAs, reducing the overall efficiency enhancement.

Table 1. Defined structural parameters of a unit cell consisting of 7×7 randomly positioned, tilted columns.

Structural parameters of nanocolumns	
Column density	4.9×10^9 cm^{-2}
Base diameter	100 nm
Top diameter	30nm
Column length	1.2 μm
Tilt angle	63.4°
Maximum position variation	36.25 nm

On the contrary, the photocurrent generated at wavelengths that are transparent to the window layer is enhanced by 42%, calculated by the integral of the product of EQE and the AM 1.5 g spectrum.[27] The enhancement is also better than a cell with a conventional SiO_2 AR coating, which is typically in the 30% range for the short-circuit current. We conclude that the superior improvement mostly originates from the enhanced transmission depicted by the uniformly distributed column profiles.

In conclusion, distinctive ITO nanocolumns grown by glancing-angle deposition have been employed as the conductive AR coating for GaAs solar cells. Ellipsometric spectroscopy and RCWA calculations verify that the material exhibits excellent AR for both s- and p-polarizations, up to an incidence angle of 70° for the wavelength range of $\lambda = 350$–900 nm. The nanostructured ITO AR layer achieves an enhancement factor of 42% for photocurrents generated at wavelengths that are transparent to the window layer, demonstrating a viable efficiency-boosting strategy for next-generation photovoltaics.

Experimental

Fabrication of the GaAs cell: In this study, the structure of a single-junction GaAs solar cell consists of a heavily doped p-type contact layer, an $Al_{0.8}Ga_{0.2}As$ window, a GaAs emitter, an n-type base, and an $Al_{0.3}Ga_{0.7}As$ back-surface-field (BSF) layer, which was epitaxially grown on an n-type GaAs substrate with a 2° off-cut by metal–organic chemical-vapor deposition (MOCVD). The top metal contact was first formed by optical lithography and e-beam evaporation, followed by the mesa definition with an area of 1 cm × 1 cm, and the deposition of the bottom contact. The exposed p-type contact layer was then removed by dipping into a solution of citric acid/H_2O_2/H_2O = 1:3:10 for 5 min. Finally, the cell was annealed at 400 °C for 1 min to form Ohmic contacts on both sides.

Calculation Method: The RCWA method is often employed to solve for the diffraction and transmission efficiency of optical diffractive elements. The reflectivity is obtained as a sum of the reflection–diffraction efficiencies of different diffraction orders. In this study, only specular reflection is dominant in calculation, as been verified in measurement. The nanostructure consisting of 7 × 7 random columns is defined as a unit cell, where periodic boundary conditions are enforced. The size of unit cell and randomness of nanopillar positions have been chosen to assure convergence. Detailed structural parameters of the nanocolumns are summarized in Table 1. The material dispersion relation is obtained by fitting the normally incident reflectivity spectrum of an ITO thin film deposited on a silicon wafer. ITO becomes absorptive at wavelengths below 400 nm. The angular and spectral reflectivities of ITO nanocolumns are then calculated using the extracted complex refractive indices.

Acknowledgements

The authors thank Prof. M. C. Lin at the Department of Chemistry, Emory University, USA for fruitful discussion. This work is founded by National Science Council in Taiwan under grant number 96-2221-E-009-095-MY3 and 97-2120-M-006-009.

Received: August 31, 2008
Revised: November 10, 2008
Published online: January 22, 2009

[1] M. A. Green, *Third Generation Photovoltaics: Advanced Solar Electricity Generation*, Springer-Verlag, Berlin **2003**, pp. 1–3.
[2] J. Zhao, A. Wang, P. Altermatt, M. A. Green, *Appl. Phys. Lett.* **1995**, *66*, 3636.
[3] J. Zhao, A. Wang, M. A. Green, F. Ferrazza, *Appl. Phys. Lett.* **1998**, *73*, 1991.
[4] D. J. Aiken, *Sol. Energy Mater. Sol. Cells* **2000**, *64*, 393.
[5] W. H. Southwell, *Opt. Lett.* **1983**, *8*, 584.
[6] A. Dobrowolski, D. Poitras, P. Ma, H. Vakil, M. Acree, *Appl. Opt.* **2002**, *41*, 3075.
[7] D. Poitras, J. A. Dobrowolski, *Appl. Opt.* **2004**, *43*, 1286.
[8] P. B. Clapham, M. C. Hutley, *Nature* **1973**, *244*, 281.
[9] P. B. Clapham, M. C. Hutley, *Opt. Acta* **1982**, *29*, 993.
[10] M. E. Motamedi, W. H. Southwell, W. J. Gunning, *Appl. Opt.* **1992**, *31*, 4371.
[11] P. Lalanne, G. M. Morris, *Nanotechnology*, **1997**, *8*, 53.
[12] Y. Kanamori, K. Hane, H. Sai, H. Yugami, *Appl. Phys. Lett.* **2001**, *78*, 142.
[13] Y. F. Huang, S. Chattopadhyay, Y. J. Jen, C. Y. Peng, T. A. Liu, Y. K. Hsu, C. L. Pan, H. C. Lo, C. H. Hsu, Y. H. Chang, C. S. Lee, K. H. Chen, L. C. Chen, *Nat. Nanotechnol.* **2007**, *2*, 770.
[14] D. S. Hobbs, R. D. Macleod, J. R. Riccobono, *Proc. SPIE* **2007**, *6545*, 65450Y.
[15] S. R. Kennedy, M. J. Brett, *Appl. Opt.* **2003**, *42*, 4573.
[16] J. Q. Xi, M. F. Schubert, J. K. Kim, E. F. Schubert, M. Chen, S. Y. Lin, W. Liu, J. A. Smart, *Nat. Photonics* **2007**, *1*, 176.
[17] J. K. Kim, S. Chhajed, M. F. Schubert, E. F. Schubert, A. J. Fischer, M. H. Crawford, J. Cho, H. Kim, C. Sone, *Adv. Mater.* **2008**, *20*, 801.
[18] S. Takaki, Y. Aoshima, R. Satoh, *Jpn. J. Appl. Phys.* **2007**, *46*, 3537.
[19] H. Yumoto, S. Onozumi, Y. Kato, M. Ishihara, K. Kishi, *Cryst. Res. Technol.* **1996**, *31*, 159.
[20] H. Yumoto, H. Hatano, T. Watanabe, K. Fujikawa, H. Sato, *Jpn. J. Appl. Phys.* **1993**, *32*, 1204.
[21] C. H. Chang, P. Yu, C. H. Chiu, H. C. Kuo, *Proceedings of the 33rd IEEE Photovoltaic Specialists Conference*, San Diego, CA, USA, **2008**, in press.
[22] C. H. Chiu, P. Yu, H. C. Kuo, C. C. Chen, T. C. Lu, S. C. Wang, S. S. Hsu, Y. J. Cheng, Y. C. Chang, *Opt. Express* **2008**, *16*, 8748.
[23] C. C. Chen, P. Yu, H. C. Kuo, *Proceedings of the 2007 IEEE/LEOS International Conference on Optical MEMS and Nanophotonics*, Hualien, Taiwan, **2007**, 107.
[24] N. Balasubrarnanian, A. Subrahrnanyarn, *J. Phys. D: Appl. Phys.* **1989**, *22*, 206.
[25] H. Kim, C. M. Gilmore, A. Piqué, J. S. Horwitz, H. Mattoussi, H. Murata, Z. H. Kafafi, D. B. Chrisey, *J. Appl. Phys.* **1999**, *86*, 6451.
[26] I. Vurgaftmana, J. R. Meyer, L. R. Ram-Mohan, *J. Appl. Phys.* **2001**, *89*, 5815.
[27] J. Nelson, *The Physics of Solar Cells*, Imperial College Press, UK **2003**, p. 29.